Accurate low-order dynamic model of a compact plate heat exchanger

authored by **A. Michel and A. Kugi**

and published in *International Journal of Heat and Mass Transfer*.

Accurate low-order dynamic model of a compact plate heat exchanger

Alexander Michel*, Andreas Kugi

Automation and Control Institute (ACIN), Vienna University of Technology, Gußhausstraße 27-29 / E376, 1040 Vienna, Austria

Abstract

This paper deals with the derivation of a low-dimensional mathematical model of a compact plate heat exchanger capturing the significant nonlinearities and the essential dynamic behavior in an accurate way. Thereby, the model is based on the basic laws of thermodynamics and the similitude theory of Nußelt. It is shown that reasonable simplifications according to the specific design and the typical operating conditions of compact plate heat exchangers together with a semi-discretization of the spatial domain by means of the finite volume method provides a compact finite-dimensional approximation of the underlying partial differential equations (pdes). In this context, two different interpolation schemes of the finite volume method are compared, i.e. a classical upwind scheme and a new concept based on an approximate stationary solution of the underlying pdes. The latter ensures high accuracy even for very low-order discretizations, which is shown by means of simulation and measurement results.

Keywords: low-order dynamic model, compact plate heat exchanger, finite volume method, global power balance

1. Introduction

Compact plate heat exchangers like small sized brazed plate heat exchangers are increasingly used in the field of district heating, heat recovery, industrial process cooling and heating, hydraulic oil cooling or cooling of machine tools. Their advantages are high heat transfer rates, a small overall size, a high resistance against fouling, high working pressures, a simple design and thus low costs in production. The working principle of all plate heat exchangers is the same, namely heat is exchanged between two fluid circuits divided by plates. Thereby a 1/1 pass flow arrangement, where the fluid paths of the two circuits are arranged in an alternating manner, is commonly used in industry [1], see Figure 1. In order to accurately track a desired outlet temperature under dynamically changing operating conditions, a model-based control design, which exploits the nonlinear structure of the heat exchanger model, has the potential to outperform the traditionally used linear control strategies. A prerequisite for the application of model-based control strategies is the derivation of an accurate low-dimensional mathematical model as a design model. Otherwise the resulting control strategies may get computationally too expensive to be implemented in real-time on a standard industrial process control unit. Therefore, we aim at developing a mathematical model of

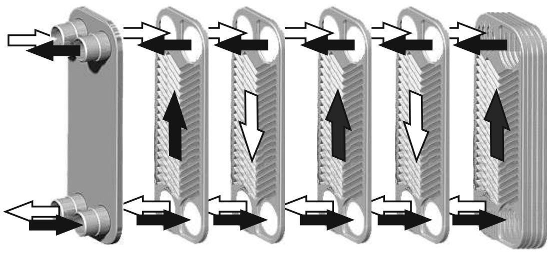

Figure 1: Design of a 1/1 pass countercurrent plate heat exchanger.

*Corresponding author: Tel.: +43 1 58801 376 21, fax: +43 1 58801 376 99

Email addresses: michel@acin.tuwien.ac.at (Alexander Michel), kugi@acin.tuwien.ac.at (Andreas Kugi)

URL: http://www.acin.tuwien.ac.at (Alexander Michel)

Postprint submitted to International Journal of Heat and Mass Transfer

Post-print version of the article: A. Michel and A. Kugi, "Accurate low-order dynamic model of a compact plate heat exchanger", *International Journal of Heat and Mass Transfer*, vol. 61, no. 33, pp. 323–331, 2013. DOI: 10.1016/j.ijheatmasstransfer.2013.01.072

The content of this post-print version is identical to the published paper but without the publisher's final layout or copy editing.

Nomenclature

A_c cross section $A_c = BH$ [m^2]
$\mathbf{A}, \mathbf{B}, \mathbf{C}, \mathbf{D}$ system matrices of system Eq. (29)
B channel width [m]
C_{Nu} correlation parameter
c_p specific heat capacity [J/(kg K)]
d_h hydraulic diameter $d_h = 2H$ [m]
H channel heigth [m]
h heat transfer coefficient [W/(m^2 K)]
H_p plate heigth [m]
k thermal conductivity [W/(m K)]
L channel length [m]
M number of volume elements
m mass [kg]
$\dot{m}$ mass flow rate [kg/s]
N_c number of channels
N_p number of plates
n_{Pr} correlation parameter
n_{Re} correlation parameter
Nu Nußelt number $Nu = hd_h/k$
Pr Prandtl number $Pr = \mu c_p/k$
$\dot{q}$ heat flux density [W/m]
Re Reynolds number $Re = |u|\varrho d_h/\mu$
t time [s]
U overall heat transfer coefficient [W/(m^2 K)]
u flow velocity [m/s]
w weighting factor
x coordinate [m]

Greek Symbols
α abbreviation (see Eq. (21)) [1/s]
β abbreviation (see Eq. (21)) [1/s]
$\varGamma$ abbreviation (see Eq. (35))
γ abbreviation (see Eqs. (33) and (34))
δ_ϑ thickness of the thermal boundary layer [m]
μ dynamic viscosity [kg/(m s)]
ϑ temperature [K]
θ temperature mean value of a volume element [K]
$\boldsymbol{\theta}$ state vector of system Eq. (29)
$\boldsymbol{\vartheta}_{\mathrm{in}}$ input vector of system Eq. (29)
$\boldsymbol{\vartheta}_{\mathrm{out}}$ output vector of system Eq. (29)
ξ linear constant parameter (see Eq. (39))
ϱ mass density [kg/m^3]

Subscripts
$1, 2, 3$ direction x_1, x_2 or x_3
I side I of the heat exchanger
II side II of the heat exchanger
f fluid
p plate
s stationary solution

Superscripts
c calculated value
in inlet
m measured value
out outlet
– (overbar) average value
∞ core flow

a plate heat exchanger, which is low-dimensional, easy to parameterize and accurate enough to capture the essential dynamics and nonlinearities.

Several mathematical models have been reported in the literature. Usually, these models consider one spatial dimension and they differ in the level of detail, especially if maldistribution of the fluid flow or the heat capacity of the plates are taken into account. Moreover, different methods for solving the underlying partial differential equations (pdes) are proposed. In [2] a mathematical model for arbitrary flow patterns is given, where the pdes are solved by means of the frequency response in the Laplace domain. Further models utilizing the Laplace transform are presented in [3, 4, 5]. An alternative approach is suggested in [6], where Galerkin's method is employed to solve the pdes. In addition, [7, 8, 9] provide mathematical models based on the finite volume method which is commonly used for numerical heat transfer problems.

Although several mathematical models are available in the literature, most of them are either high-dimensional or give a rather inaccurate approximation of the nonlinear dynamic behavior. In this context, the specific design and the typical operating conditions of compact plate heat exchangers remain mostly disregarded.

In this paper, an accurate low-order dynamic model of a 1/1 pass compact plate heat exchanger is derived in a systematic way. Thereby, the mathematical model is systematically simplified by exploiting the specific design and the typical operating conditions of compact plate heat exchangers. Starting with the basic equations of heat transfer all assumptions and simplifications being made are thoroughly explained in order to clarify the validity range of the resulting low-order dynamic model. The paper is organized as follows: In Section 2, the physical fundamentals of heat exchanger design are summarized. Based on the special design and the typical operating conditions of compact plate heat exchangers, in Section 3, specific simplifications are made to deduce a distributed-parameter model consisting of three pdes. Furthermore, a semi-discretization of the spatial domain is performed by means of the finite volume method which gives rise to a compact low-order model of only three ordinary dif-

Post-print version of the article: A. Michel and A. Kugi, "Accurate low-order dynamic model of a compact plate heat exchanger", *International Journal of Heat and Mass Transfer*, vol. 61, no. 33, pp. 323–331, 2013. DOI: 10.1016/j.ijheatmasstransfer.2013.01.072

ferential equations. Thereby, two different interpolation schemes are used, a classical upwind scheme and a new concept based on the approximate stationary global power balance. Finally, simulation and measurement results for different industrial compact plate heat exchangers demonstrate the accuracy of the proposed model. The last section, Section 5, contains some conclusions.

2. Physics of heat exchanger modeling

Figure 1 shows the basic design of the considered 1/1 pass compact plate heat exchanger. The fluid flow pas-

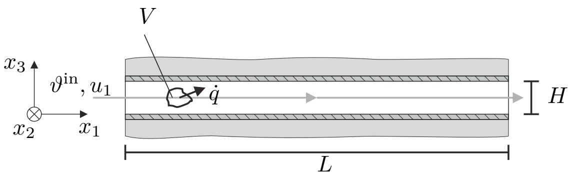

Figure 2: Channel with a simplified geometry.

sages are formed by gaps between two adjacent plates which have typically a chevron or herringbone corrugation pattern [10]. In the following, typical assumptions in heat exchanger analysis are supposed [7, 11, 12]:

1. The increase of temperature due to friction is negligible.
2. The fluid is assumed to be incompressible.
3. There are neither heat sources nor heat sinks inside a channel.
4. The heat exchange with the environment is negligible.
5. The herringbone corrugation patterns induce high vorticities and turbulences in the fluids even for low Reynolds numbers.
6. The fluid velocity in the main flow direction is high enough to justify that heat conduction along the flow direction can be neglected compared to heat convection.
7. No phase changes of the fluid occur inside the heat exchanger.

In a first step, the impact of the velocity field on the temperature is discussed before the temperature field of one channel of the plate heat exchanger is derived. In a second step, the thermal coupling between the channels will be determined. For this, a simplified geometry of a channel is considered, see Figure 2, where L, B and H refer to the effective values of the channel length, the channel width and the channel height.

Consider a small volume V inside the channel. If no phase changes occur and the material parameters are constant inside the volume V, the temperature field $\vartheta_f(x_1, x_2, x_3, t)$ inside V can be written as [13]

$$\varrho c_p \left(\frac{\partial \vartheta_f}{\partial t} + \sum_{i=1}^{3} u_i \frac{\partial \vartheta_f}{\partial x_i} \right) = - \sum_{i=1}^{3} \frac{\partial \dot{q}_i}{\partial x_i} \; , \tag{1}$$

with the velocity field $u_i(x_1, x_2, x_3, t)$, $i = 1, \ldots, 3$ and suitable boundary and initial conditions. The left hand side of Eq. (1) describes the convective heat flux density. Herein ϱ denotes the mass density and c_p is the specific heat capacity of the fluid. Moreover, the right hand side of Eq. (1) characterizes the heat transport over the boundary of V.

2.1. Temperature field of a channel

In order to calculate the temperature field $\vartheta_f(x_1, x_2, x_3, t)$ inside the volume V, the velocity field $u_i(x_1, x_2, x_3, t)$ has to be known. An accurate model of the velocity field yields a nonlinear system of pdes depending on the exact geometry of the plates. This entails high-order models which cannot be used for controller design. However, the assumption of a turbulent fluid flow justifies the use of a plug flow model which divides the flow in a core flow with a constant flow velocity in x_1-direction $u_1^\infty(t)$ and a velocity boundary layer [14]. This plug flow directly influences the evolving temperature field ϑ_f, which again is assumed to be composed of a thermal core and a boundary layer, see Figure 3, whereby the thickness of the thermal boundary layer δ_ϑ is negligible compared to the thickness of the thermal core. Inside the thermal core, due to the high turbulences of the fluid flow, the temperature can be considered homogeneous, that is

$$\vartheta_f(x_1, x_2, x_3, t) = \vartheta_f^\infty(x_1, t) \tag{2}$$

and

$$\frac{\partial \vartheta_f}{\partial x_2} = \frac{\partial \vartheta_f}{\partial x_3} = 0 \; . \tag{3}$$

Thus, integrating Eq. (1) over the cross section $A_c = BH$ we get

$$\begin{aligned} &\int_0^B \int_0^H \varrho c_p \left(\frac{\partial \vartheta_f}{\partial t} + \sum_{i=1}^{3} u_i \frac{\partial \vartheta_f}{\partial x_i} \right) \mathrm{d}x_2 \mathrm{d}x_3 \\ &= - \int_0^B \int_0^H \sum_{i=1}^{3} \frac{\partial \dot{q}_i}{\partial x_i} \mathrm{d}x_2 \mathrm{d}x_3 \; . \end{aligned} \tag{4}$$

Because the thickness of the boundary layer δ_ϑ is considerably small compared to the height of the channel H, the energy stored in the boundary layer will be neglected. Furthermore, the heat fluxes $\dot{q}_1, \dot{q}_2$ can also be considered zero due to the assumptions that the fluid is ideally mixed (cf. Eqs. (2) and (3)), no heat exchange takes place with the environment and that there is no heat conduction along x_1-direction. Thus, the mathematical model of the temperature field in a channel of a plate heat exchanger according to Eq. (4) simplifies to

$$A_c \varrho c_p \left(\frac{\partial \vartheta}{\partial t} + u \frac{\partial \vartheta}{\partial x_1} \right) = -B \dot{q}_3 \Big|_{x_3=0}^{x_3=H} \tag{5}$$

Post-print version of the article: A. Michel and A. Kugi, "Accurate low-order dynamic model of a compact plate heat exchanger", *International Journal of Heat and Mass Transfer*, vol. 61, no. 33, pp. 323–331, 2013. DOI: 10.1016/j.ijheatmasstransfer.2013.01.072

with the boundary conditions

$$\begin{cases} \vartheta(0,t) = \vartheta^{\text{in}} & \text{for} \quad u \geq 0 \\ \vartheta(L,t) = \vartheta^{\text{in}} & \text{for} \quad u < 0 \end{cases} \tag{6}$$

and appropriate initial conditions. Note that for the sake of readability in Eq. (5) and henceforth ϑ_f^∞ is replaced by ϑ and u_1^∞ by u, respectively. Moreover, ϑ^{in} denotes the inlet temperature in the channel.

2.2. Thermal coupling of neighboring channels

In order to model the thermal coupling between neighboring channels, a plate of height H_p exposed to two fluids of different core temperatures $\vartheta_{\text{I}} > \vartheta_{\text{II}}$ and fluid velocities $u_{\text{I}}, u_{\text{II}}$ is considered, see Figure 3. As it is shown in

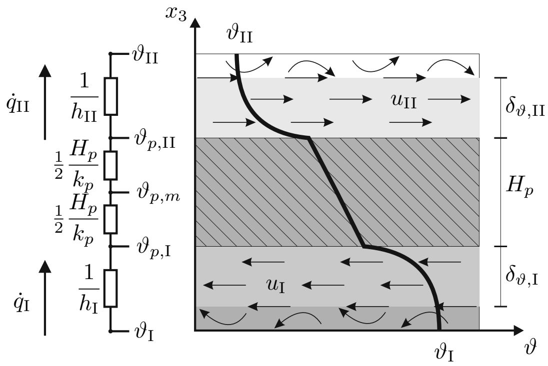

Figure 3: Schematics of the heat transfer between two adjacent channels.

Figure 3, heat is transferred from the core flow of fluid I through the boundary layer to the plate and then to fluid II. A common way to describe this kind of convective heat transfer is to introduce a so-called heat transfer coefficient h, which allows to calculate the transferred heat flux between fluid I and the plate by means of Newton's law of cooling in the form

$$\dot{q}_{\text{I}} = h_{\text{I}} \left(\vartheta_{\text{I}} - \vartheta_{p,\text{I}}\right) \ , \tag{7}$$

where $\vartheta_{p,\text{I}}$ denotes the temperature of the wall in contact with fluid I. In an analogous way the heat flux $\dot{q}_{\text{II}}$ reads as

$$\dot{q}_{\text{II}} = h_{\text{II}} \left(\vartheta_{p,\text{II}} - \vartheta_{\text{II}}\right) \ . \tag{8}$$

It is well known that an analytical expression for the heat transfer coefficient h is only available for very simplistic scenarios. In the general case the calculation of h requires an accurate knowledge of the fluid velocity field which in turn leads to high-order models with high computational effort. Therefore, semi-empirical methods like the similitude theory according to Nußelt are often employed in the design of heat exchangers. Basically, the latter approach relies on a suitable approximation of the functional dependence of the Nußelt number Nu, on the Prandtl number Pr and the Reynolds number Re [14], i.e.,

$$Nu = f_{Nu}(Pr, Re) \tag{9}$$

with

$$Nu = \frac{h d_h}{k} \ , \qquad Pr = \frac{\mu c_p}{k} \ , \qquad Re = \frac{|u| \varrho d_h}{\mu} \ , \tag{10}$$

where $d_h = 2H$ denotes the hydraulic diameter, k is the fluid thermal conductivity and μ the dynamic viscosity. In recent years, several relations for the Nußelt correlation Eq. (9) of plate heat exchangers have been reported in the literature, see, e.g., [15, 16, 17, 18]. It is common practice to assume that the Nußelt number Nu is constant along the flow direction where the material parameters k, μ, c_p and ϱ are evaluated at the average temperature of inlet ϑ^{in} and outlet ϑ^{out}. According to [17] the Nußelt number for compact plate heat exchangers can be expressed in the form

$$Nu = C_{Nu} Pr^{n_{Pr}} Re^{n_{Re}} \ , \tag{11}$$

with the constant empirical parameters C_{Nu}, n_{Pr} and n_{Re} which have to be determined by means of suitable experiments. By combining Eq. (10) and Eq. (11) the heat transfer coefficients h_{I} and h_{II} can be calculated which solely depend on $\vartheta_{\text{I}}^{\text{in}}$, $\vartheta_{\text{I}}^{\text{out}}$, u_{I} and $\vartheta_{\text{II}}^{\text{in}}$, $\vartheta_{\text{II}}^{\text{out}}$, u_{II}, respectively.

Analogous to Eq. (1) the temperature field $\vartheta_p(x_1, x_2, x_3, t)$ of the plate satisfies the pde

$$\varrho_p c_{p,p} \frac{\partial \vartheta_p}{\partial t} = -\sum_{i=1}^{3} \frac{\partial \dot{q}_i}{\partial x_i} \tag{12}$$

with appropriate boundary and initial conditions. Henceforth, in x_2-direction the plate temperature is assumed to be homogenous and boundary effects are neglected, i.e. $\dot{q}_2 = 0$. Moreover, since the height H_p of a typical plate is rather small and the thermal conductivity k_p of metal is large, the temperature profile in x_3-direction can be considered in a quasi-stationary manner. Utilizing Fourier's law of heat conduction in x_1-direction, see, e.g., [15]

$$\dot{q}_1 = k_p \frac{\partial \vartheta_p}{\partial x_1} \tag{13}$$

and integrating Eq. (12) over the cross section $A_{c,p} = B H_p$ of the plate yields

$$\varrho_p c_{p,p} B \int_0^{H_p} \frac{\partial \vartheta_p}{\partial t} \mathrm{d}x_3 = -k_p B \int_0^{H_p} \frac{\partial^2 \vartheta_p}{\partial x_1^2} \mathrm{d}x_3 - B \ \dot{q}_3 \big|_{x_3=0}^{x_3=H_p} \ . \tag{14}$$

The stationarity assumption in x_3-direction implies (see Figure 3)

$$\frac{1}{H_p} \int_0^{H_p} \vartheta_p \mathrm{d}x_3 = \frac{1}{2} \left(\vartheta_{p,\text{I}} + \vartheta_{p,\text{II}}\right) := \vartheta_{p,m} \tag{15}$$

Post-print version of the article: A. Michel and A. Kugi, "Accurate low-order dynamic model of a compact plate heat exchanger", *International Journal of Heat and Mass Transfer*, vol. 61, no. 33, pp. 323–331, 2013. DOI: 10.1016/j.ijheatmasstransfer.2013.01.072
The content of this post-print version is identical to the published paper but without the publisher's final layout or copy editing.

and thus Eq. (14) can be written in the form

$$\varrho_p c_{p,p} A_{c,p} \frac{\partial \vartheta_{p,m}}{\partial t} = -\, A_{c,p} k_p \frac{\partial^2 \vartheta_{p,m}}{\partial x_1^2} + B\left(\dot{q}_{\mathrm{I}} - \dot{q}_{\mathrm{II}}\right) \ , \quad (16)$$

with the boundary conditions (no heat exchange with the environment)

$$\left.\frac{\partial \vartheta_{p,m}}{\partial x_1}\right|_{x_1=0} = \left.\frac{\partial \vartheta_{p,m}}{\partial x_1}\right|_{x_1=L} = 0 \quad (17)$$

and suitable initial conditions. Note that $\vartheta_{p,m}$ is exactly the temperature in the middle of the plate, i.e. for $x_3 = H_p/2$, and the heat fluxes $\dot{q}_{\mathrm{I}}$ and $\dot{q}_{\mathrm{II}}$ correspond to Eqs. (7) and (8).

In view of the stationary temperature profile in x_3-direction, the surface plate temperatures $\vartheta_{p,\mathrm{I}}$ and $\vartheta_{p,\mathrm{II}}$ can be expressed as

$$\vartheta_{p,\mathrm{I}} = \vartheta_{p,m} + \frac{1}{2}\frac{H_p}{k_p}\dot{q}_{\mathrm{I}} \ , \quad (18a)$$

$$\vartheta_{p,\mathrm{II}} = \vartheta_{p,m} - \frac{1}{2}\frac{H_p}{k_p}\dot{q}_{\mathrm{II}} \ . \quad (18b)$$

Substituting Eq. (18) into Eqs. (7) and (8) and solving with respect to the heat fluxes results in

$$\dot{q}_{\mathrm{I}} = h_{p,\mathrm{I}}\left(\vartheta_{\mathrm{I}} - \vartheta_{p,m}\right), \qquad \frac{1}{h_{p,\mathrm{I}}} = \frac{1}{h_{\mathrm{I}}} + \frac{1}{2}\frac{H_p}{k_p} \ , \quad (19a)$$

$$\dot{q}_{\mathrm{II}} = h_{p,\mathrm{II}}\left(\vartheta_{p,m} - \vartheta_{\mathrm{II}}\right), \qquad \frac{1}{h_{p,\mathrm{II}}} = \frac{1}{h_{\mathrm{II}}} + \frac{1}{2}\frac{H_p}{k_p} \ . \quad (19b)$$

The thermal equivalent network of Eq. (19) is depicted on the left hand side of Figure 3.

3. Compact plate heat exchanger model

The temperature field of every fluid channel can be modeled by Eq. (5) and the temperature field of every plate by Eq. (16). Furthermore, the heat flux $\dot{q}_3$ characterizing the thermal coupling of the fluid with a plate is given by Eq. (19). The resulting model of a plate heat exchanger with N_p plates thus consists of $2N_p - 1$ nonlinear pdes. In particular for large number of plates this model is not suitable for model-based control design. However, in the derivation of the mathematical model the specific design and the typical operating conditions of compact plate heat exchangers have been disregarded so far. As it will be shown in the sequel, the consideration of these conditions not only reduces the number of pdes, but also allows for an accurate low-order approximation of the spatial domain. In this context the following simplifications are made:

Due to the small volume of the gatherer, (i) the transport time as well as the (ii) pressure drop inside the gatherer is negligible. This in turn suggest to assume that (iii) the inlet temperature and (iv) the fluid velocity of every channel with the same fluid are equal. The latter implies that no maldistribution of flow occurs which has already been shown for typical compact heat exchangers in [17]. In addition, due to the design with equal plates, (v) the cross section A_c and (vi) the heat transfer coefficients h_p of every channel passed through by the same fluid are equal, see Eq. (19). Furthermore, the small overall volumes of both sides (I and II) together with the high flow rates of the fluids lead to a (vii) low residence time of the fluids in each channel.

Due to the same inlet temperatures, fluid flows and geometric parameters of each channel of fluid I and II, locally the same temperature distribution evolves in flow direction. This suggests to describe the temperature distribution of each channel of the same fluid by only one average temperature distribution $\bar{\vartheta}$ and thus reduce the model from $2N_p - 1$ pdes to only 3 pdes. Henceforth, the index I (II) always refers to parameters of a channel with fluid I (II) and the index p indicates parameters of a plate. In order to determine the average model, we introduce the effective heat transfer area $BL\,(N_p - 2)$ for both fluids and the effective cross section of fluid I and fluid II, given by $A_{c,\mathrm{I}} = N_{c,\mathrm{I}} A_c$ and $A_{c,\mathrm{II}} = N_{c,\mathrm{II}} A_c$, respectively. Thereby, $N_{c,\mathrm{I}}$ ($N_{c,\mathrm{II}}$) denotes the total number of parallel channels with fluid I (II), with $N_{c,\mathrm{I}} + N_{c,\mathrm{II}} = N_p - 1$. Thus, the mathematical model of the compact plate heat exchanger with the local average temperature distribution $\bar{\vartheta}_{\mathrm{I}}$ and $\bar{\vartheta}_{\mathrm{II}}$ of fluid I and II and the local average plate temperature distribution $\bar{\vartheta}_p$ results from Eqs. (5), (16) and (19) in the form

$$\frac{\partial \bar{\vartheta}_{\mathrm{I}}}{\partial t} = -\, u_{\mathrm{I}} \frac{\partial \bar{\vartheta}_{\mathrm{I}}}{\partial x_1} - \alpha_{\mathrm{I}}\left(\bar{\vartheta}_{\mathrm{I}} - \bar{\vartheta}_p\right) \quad (20a)$$

$$\frac{\partial \bar{\vartheta}_p}{\partial t} = -\, \frac{k_p}{c_{p,p}\varrho_p}\frac{\partial^2 \bar{\vartheta}_p}{\partial x_1^2} - \beta_{\mathrm{I}}\left(\bar{\vartheta}_p - \bar{\vartheta}_{\mathrm{I}}\right) - \beta_{\mathrm{II}}\left(\bar{\vartheta}_p - \bar{\vartheta}_{\mathrm{II}}\right) \quad (20b)$$

$$\frac{\partial \bar{\vartheta}_{\mathrm{II}}}{\partial t} = -\, u_{\mathrm{II}} \frac{\partial \bar{\vartheta}_{\mathrm{II}}}{\partial x_1} - \alpha_{\mathrm{II}}\left(\bar{\vartheta}_{\mathrm{II}} - \bar{\vartheta}_p\right) \quad (20c)$$

with the abbreviations

$$\alpha_i = \frac{h_{p,i}}{H\varrho_i c_{p,i}}\frac{N_p - 2}{N_{c,i}} \ , \qquad \beta_i = \frac{2h_{p,i}}{H_p \varrho_p c_{p,p}} \ , \qquad i \in \{\mathrm{I}, \mathrm{II}\} \ , \quad (21)$$

the boundary conditions

$$\begin{cases} \bar{\vartheta}_{\mathrm{I}}(0,t) = \vartheta_{\mathrm{I}}^{\mathrm{in}} & \text{for} \quad u_{\mathrm{I}} \geq 0 \\ \bar{\vartheta}_{\mathrm{I}}(L,t) = \vartheta_{\mathrm{I}}^{\mathrm{in}} & \text{for} \quad u_{\mathrm{I}} < 0 \end{cases} \quad (22a)$$

$$\begin{cases} \bar{\vartheta}_{\mathrm{II}}(0,t) = \vartheta_{\mathrm{II}}^{\mathrm{in}} & \text{for} \quad u_{\mathrm{II}} \geq 0 \\ \bar{\vartheta}_{\mathrm{II}}(L,t) = \vartheta_{\mathrm{II}}^{\mathrm{in}} & \text{for} \quad u_{\mathrm{II}} < 0 \end{cases} \quad (22b)$$

$$\left.\frac{\partial \bar{\vartheta}_p}{\partial x_1}\right|_{x_1=0} = \left.\frac{\partial \bar{\vartheta}_p}{\partial x_1}\right|_{x_1=L} = 0 \quad (22c)$$

and the channel velocities

$$u_{\mathrm{I}} = \frac{\dot{m}_{\mathrm{I}}}{\varrho_{\mathrm{I}} A_{c,\mathrm{I}}} \quad \text{and} \quad u_{\mathrm{II}} = \frac{\dot{m}_{\mathrm{II}}}{\varrho_{\mathrm{II}} A_{c,\mathrm{II}}} \ . \quad (23)$$

Post-print version of the article: A. Michel and A. Kugi, "Accurate low-order dynamic model of a compact plate heat exchanger", *International Journal of Heat and Mass Transfer*, vol. 61, no. 33, pp. 323–331, 2013. DOI: 10.1016/j.ijheatmasstransfer.2013.01.072

Here $\dot{m}_{\mathrm{I}}$ and $\dot{m}_{\mathrm{II}}$ denote the overall mass flow rates of fluid I and II passing through the heat exchanger. In the next step the distributed-parameter system of Eq. (20) is spatially discretized in order to obtain a system of ordinary differential equations (odes). It is common practice to approximate hyperbolic pdes as Eq. (20) by means of the finite volume method, see, e.g., [19, 20, 21]. For this, the particular control volume is partitioned in M equally spaced volume elements of length $\frac{L}{M}$. Then Eq. (20) is integrated over the whole volume, where the integral is divided into a sum of integrals over the partitioned elements, which results in

$$\sum_{j=1}^{M} \frac{L}{M}\frac{\mathrm{d}\theta_{j,\mathrm{I}}}{\mathrm{d}t} + \frac{\dot{m}_{\mathrm{I}}}{\varrho_{\mathrm{I}} A_{c,\mathrm{I}}} \left.\bar{\vartheta}_{\mathrm{I}}\right|_{x_1=(j-1)\frac{L}{M}}^{x_1=j\frac{L}{M}} + \frac{L}{M}\alpha_{\mathrm{I}}\left(\theta_{j,\mathrm{I}} - \theta_{j,p}\right) = 0 \tag{24a}$$

$$\sum_{j=1}^{M} \frac{L}{M}\frac{\mathrm{d}\theta_{j,p}}{\mathrm{d}t} + \frac{k_p}{c_{p,p}\varrho_p} \left.\frac{\partial \bar{\vartheta}_p}{\partial x_1}\right|_{x_1=(j-1)\frac{L}{M}}^{x_1=j\frac{L}{M}} + \frac{L}{M}\beta_{\mathrm{I}}\left(\theta_{j,p} - \theta_{j,\mathrm{I}}\right) + \frac{L}{M}\beta_{\mathrm{II}}\left(\theta_{j,p} - \theta_{j,\mathrm{II}}\right) = 0 \tag{24b}$$

$$\sum_{j=1}^{M} \frac{L}{M}\frac{\mathrm{d}\theta_{j,\mathrm{II}}}{\mathrm{d}t} + \frac{\dot{m}_{\mathrm{II}}}{\varrho_{\mathrm{II}} A_{c,\mathrm{II}}} \left.\bar{\vartheta}_{\mathrm{II}}\right|_{x_1=(j-1)\frac{L}{M}}^{x_1=j\frac{L}{M}} + \frac{L}{M}\alpha_{\mathrm{II}}\left(\theta_{j,\mathrm{II}} - \theta_{j,p}\right) = 0 \ . \tag{24c}$$

Thereby, the temperature mean values of the different volume elements

$$\theta_{j,i} = \frac{M}{L}\int_{(j-1)\frac{L}{M}}^{j\frac{L}{M}} \bar{\vartheta}_i \mathrm{d}x_1 \qquad i \in \{\mathrm{I}, \mathrm{II}, p\} \tag{25}$$

are introduced as new state variables of the mathematical model. Since not only the three sums in Eqs. (24a), (24b) and (24c) must vanish, but also its summands, this results in a finite-dimensional model of $3M$ ordinary differential equations (odes). In general, the choice of the number of volume elements M has a great impact on the dynamic behavior of the resulting finite-dimensional model, especially on the approximation of the transport phenomena. However, as will be seen in Section 4, due to typical operating conditions of compact plate heat exchangers with low residence time and limited dynamics of the inlet temperatures the transport phenomena are less dominant. This allows to model the heat exchanger by means of only three odes.

For $M = 1$ the diffusion term in Eq. (24b)

$$\left.\frac{\partial \bar{\vartheta}_p}{\partial x_1}\right|_{x_1=(j-1)\frac{L}{M}}^{x_1=j\frac{L}{M}} = 0 \tag{26}$$

vanishes due to the boundary conditions of Eq. (22c), the average temperatures at the element border in Eqs. (24a) and (24c) simplify to

$$\frac{\dot{m}_i}{\varrho_i A_{c,i}} \left.\bar{\vartheta}_i\right|_{x_1=0}^{x_1=L} = |\dot{m}_i| \frac{1}{\varrho_i A_{c,i}} \left(\vartheta_i^{\mathrm{out}} - \vartheta_i^{\mathrm{in}}\right) \tag{27}$$

with $i \in \{\mathrm{I}, \mathrm{II}\}$ and Eq. (24) takes the form

$$\frac{\mathrm{d}\theta_{\mathrm{I}}}{\mathrm{d}t} = -\frac{|\dot{m}_{\mathrm{I}}|}{m_{\mathrm{I}}}\left(\vartheta_{\mathrm{I}}^{\mathrm{out}} - \vartheta_{\mathrm{I}}^{\mathrm{in}}\right) - \alpha_{\mathrm{I}}\left(\theta_{\mathrm{I}} - \theta_p\right) \tag{28a}$$

$$\frac{\mathrm{d}\theta_p}{\mathrm{d}t} = -\beta_{\mathrm{I}}\left(\theta_p - \theta_{\mathrm{I}}\right) - \beta_{\mathrm{II}}\left(\theta_p - \theta_{\mathrm{II}}\right) \tag{28b}$$

$$\frac{\mathrm{d}\theta_{\mathrm{II}}}{\mathrm{d}t} = -\frac{|\dot{m}_{\mathrm{II}}|}{m_{\mathrm{II}}}\left(\vartheta_{\mathrm{II}}^{\mathrm{out}} - \vartheta_{\mathrm{II}}^{\mathrm{in}}\right) - \alpha_{\mathrm{II}}\left(\theta_{\mathrm{II}} - \theta_p\right) \ , \tag{28c}$$

where $m_{\mathrm{I}} = \varrho_{\mathrm{I}} A_{c,\mathrm{I}} L$ and $m_{\mathrm{II}} = \varrho_{\mathrm{II}} A_{c,\mathrm{II}} L$ denote the total mass inside the heat exchanger of fluid I and fluid II, respectively. The next step is to determine a relationship between the outlet temperatures $\vartheta_{\mathrm{I}}^{\mathrm{out}}$ and $\vartheta_{\mathrm{II}}^{\mathrm{out}}$ and the state variables θ_{I}, θ_{II}, and θ_p. It will be shown that the overall model can be written in the compact form

$$\frac{\mathrm{d}}{\mathrm{d}t}\boldsymbol{\theta} = \mathbf{A}(\dot{\mathbf{m}})\boldsymbol{\theta} + \mathbf{B}(\dot{\mathbf{m}})\boldsymbol{\vartheta}_{\mathrm{in}} \tag{29a}$$

$$\boldsymbol{\vartheta}_{\mathrm{out}} = \mathbf{C}(\dot{\mathbf{m}})\boldsymbol{\theta} + \mathbf{D}(\dot{\mathbf{m}})\boldsymbol{\vartheta}_{\mathrm{in}} \tag{29b}$$

with the state vector $\boldsymbol{\theta} = [\theta_{\mathrm{I}}, \theta_p, \theta_{\mathrm{II}}]^T$, the input vectors $\dot{\mathbf{m}} = [\dot{m}_{\mathrm{I}}, \dot{m}_{\mathrm{II}}]^T$ and $\boldsymbol{\vartheta}_{\mathrm{in}} = \left[\vartheta_{\mathrm{I}}^{\mathrm{in}}, \vartheta_{\mathrm{II}}^{\mathrm{in}}\right]^T$, the output vector $\boldsymbol{\vartheta}_{\mathrm{out}} = \left[\vartheta_{\mathrm{I}}^{\mathrm{out}}, \vartheta_{\mathrm{II}}^{\mathrm{out}}\right]^T$ and appropriate initial conditions.

3.1. Upwind scheme

One of the simplest approximation schemes in the finite volume method is the so-called upwind scheme, where the outlet temperatures are interpolated in the form [20]

$$\vartheta_i^{\mathrm{out}} = \theta_i \ , \qquad i \in \{\mathrm{I}, \mathrm{II}\} \ . \tag{30}$$

Applying the upwind scheme to Eq. (28) the system matrices of Eq. (29) read as

$$\mathbf{A} = \begin{bmatrix} -\frac{|\dot{m}_{\mathrm{I}}|}{m_{\mathrm{I}}} - \alpha_{\mathrm{I}} & \alpha_{\mathrm{I}} & 0 \\ \beta_{\mathrm{I}} & -\left(\beta_{\mathrm{I}} + \beta_{\mathrm{II}}\right) & \beta_{\mathrm{II}} \\ 0 & \alpha_{\mathrm{II}} & -\frac{|\dot{m}_{\mathrm{II}}|}{m_{\mathrm{II}}} - \alpha_{\mathrm{II}} \end{bmatrix} ,$$
$$\mathbf{B} = \begin{bmatrix} \frac{|\dot{m}_{\mathrm{I}}|}{m_{\mathrm{I}}} & 0 \\ 0 & 0 \\ 0 & \frac{|\dot{m}_{\mathrm{II}}|}{m_{\mathrm{II}}} \end{bmatrix} , \quad \mathbf{C} = \begin{bmatrix} 1 & 0 & 0 \\ 0 & 0 & 1 \end{bmatrix} , \tag{31}$$
$$\mathbf{D} = \begin{bmatrix} 0 & 0 \\ 0 & 0 \end{bmatrix} .$$

Note that α_i and β_i, $i \in \{\mathrm{I}, \mathrm{II}\}$, depend on the mass flow rates in a nonlinear manner, cf. Eqs. (10), (11), (21) and (23). The upwind scheme is quite simple and leads to a compact mathematical model but has the drawback of rather high approximation errors, as will be seen in Section 4. Of course, the accuracy of the model could be improved by increasing the number of volume elements M. However, this contradicts the desire to derive low-order models which serve as a basis for optimization and real-time nonlinear control. Therefore, an alternative approach for the interpolation of the outlet temperatures based on considerations of the stationary behavior of the heat exchanger will be applied in the following.

Post-print version of the article: A. Michel and A. Kugi, "Accurate low-order dynamic model of a compact plate heat exchanger", *International Journal of Heat and Mass Transfer*, vol. 61, no. 33, pp. 323–331, 2013. DOI: 10.1016/j.ijheatmasstransfer.2013.01.072

3.2. Power balance scheme

For the subsequent derivation of the stationary temperature profiles the heat conduction of the plates in x_1-direction will be neglected, i.e. $k_p = 0$ in Eq. (20). In fact numerical calculations have shown that this term only marginally influences the results and only with this simplification an analytical solution is made possible.

Assuming countercurrent flow with $\dot{m}_{\mathrm{I}} > 0$ and $\dot{m}_{\mathrm{II}} < 0$ the boundary conditions are given by $\bar{\vartheta}_{\mathrm{I},s}(0) = \vartheta^{\mathrm{in}}_{\mathrm{I},s}$ and $\bar{\vartheta}_{\mathrm{II},s}(L) = \vartheta^{\mathrm{in}}_{\mathrm{II},s}$ and the stationary solution of Eq. (20), subsequently referred to with the index s, for $k_p = 0$ reads as

$$\bar{\vartheta}_{\mathrm{I},s}(x_1) = \vartheta^{\mathrm{in}}_{\mathrm{I},s} - \left(\vartheta^{\mathrm{in}}_{\mathrm{I},s} - \vartheta^{\mathrm{in}}_{\mathrm{II},s}\right) \frac{1 - \exp\left(-\Gamma \frac{x_1}{L}\right)}{1 + \frac{\gamma_{\mathrm{II}}}{\gamma_{\mathrm{I}}} \exp(-\Gamma)} \tag{32a}$$

$$\bar{\vartheta}_{\mathrm{II},s}(x_1) = \vartheta^{\mathrm{in}}_{\mathrm{I},s} - \left(\vartheta^{\mathrm{in}}_{\mathrm{I},s} - \vartheta^{\mathrm{in}}_{\mathrm{II},s}\right) \frac{1 + \frac{\gamma_{\mathrm{II}}}{\gamma_{\mathrm{I}}} \exp\left(-\Gamma \frac{x_1}{L}\right)}{1 + \frac{\gamma_{\mathrm{II}}}{\gamma_{\mathrm{I}}} \exp(-\Gamma)} , \tag{32b}$$

with the abbreviations

$$\gamma_{\mathrm{I}} = \frac{U (N_p - 2) BL}{c_{p,\mathrm{I}} \dot{m}_{\mathrm{I}}} , \tag{33}$$

$$\gamma_{\mathrm{II}} = \frac{U (N_p - 2) BL}{c_{p,\mathrm{II}} \dot{m}_{\mathrm{II}}} , \tag{34}$$

$$\Gamma = \gamma_{\mathrm{I}} + \gamma_{\mathrm{II}} \tag{35}$$

and the overall heat transfer coefficient

$$\frac{1}{U} = \frac{1}{h_{p,\mathrm{I}}} + \frac{1}{h_{p,\mathrm{II}}} . \tag{36}$$

Thus, the stationary outlet temperatures can be directly inferred from Eq. (32) in the form $\vartheta^{\mathrm{out}}_{\mathrm{I},s} = \bar{\vartheta}_{\mathrm{I},s}(L)$ and $\vartheta^{\mathrm{out}}_{\mathrm{II},s} = \bar{\vartheta}_{\mathrm{II},s}(0)$. It can be easily seen that the stationary temperature mean values (cf. Eq. (25) for $M = 1$)

$$\theta_{i,s} = \frac{1}{L} \int_0^L \bar{\vartheta}_{i,s} \mathrm{d}x_1 , \quad i \in \{\mathrm{I}, \mathrm{II}\} \tag{37}$$

are bounded from below and above, for instance for $\vartheta^{\mathrm{in}}_{\mathrm{I},s} > \vartheta^{\mathrm{in}}_{\mathrm{II},s}$ we have

$$\vartheta^{\mathrm{in}}_{\mathrm{I},s} \geq \theta_{\mathrm{I},s} \geq \vartheta^{\mathrm{out}}_{\mathrm{I},s} , \tag{38a}$$

$$\vartheta^{\mathrm{in}}_{\mathrm{II},s} \leq \theta_{\mathrm{II},s} \leq \vartheta^{\mathrm{out}}_{\mathrm{II},s} . \tag{38b}$$

The latter guarantees the existence of constant parameters $\xi_{\mathrm{I}}, \xi_{\mathrm{II}} \in [0, 1]$ such that the following relations

$$\theta_{\mathrm{I},s} = \vartheta^{\mathrm{in}}_{\mathrm{I},s} + \xi_{\mathrm{I}} \left(\vartheta^{\mathrm{out}}_{\mathrm{I},s} - \vartheta^{\mathrm{in}}_{\mathrm{I},s}\right) , \tag{39a}$$

$$\theta_{\mathrm{II},s} = \vartheta^{\mathrm{in}}_{\mathrm{II},s} + \xi_{\mathrm{II}} \left(\vartheta^{\mathrm{out}}_{\mathrm{II},s} - \vartheta^{\mathrm{in}}_{\mathrm{II},s}\right) \tag{39b}$$

are satisfied. Inserting Eq. (32) into Eq. (37) and then into Eq. (39), ξ_{I} and ξ_{II} can be calculated in the form

$$\xi_{\mathrm{I}} = \frac{\exp(\Gamma)(\Gamma - 1) + 1}{\Gamma (\exp(\Gamma) - 1)} , \quad \xi_{\mathrm{II}} = 1 - \xi_{\mathrm{I}} . \tag{40}$$

Remark: For cocurrent flow with $\dot{m}_{\mathrm{I}} > 0$ and $\dot{m}_{\mathrm{II}} > 0$, $\bar{\vartheta}_{\mathrm{I},s}(0) = \vartheta^{\mathrm{in}}_{\mathrm{I},s}$ and $\bar{\vartheta}_{\mathrm{II},s}(0) = \vartheta^{\mathrm{in}}_{\mathrm{II},s}$ similar expressions can be derived for the stationary solution

$$\bar{\vartheta}_{\mathrm{I},s}(x_1) = \vartheta^{\mathrm{in}}_{\mathrm{I},s} - \gamma_{\mathrm{I}} \left(\vartheta^{\mathrm{in}}_{\mathrm{I},s} - \vartheta^{\mathrm{in}}_{\mathrm{II},s}\right) \frac{1 - \exp\left(-\Gamma \frac{x_1}{L}\right)}{\Gamma} , \tag{41a}$$

$$\bar{\vartheta}_{\mathrm{II},s}(x_1) = \vartheta^{\mathrm{in}}_{\mathrm{II},s} + \gamma_{\mathrm{II}} \left(\vartheta^{\mathrm{in}}_{\mathrm{I},s} - \vartheta^{\mathrm{in}}_{\mathrm{II},s}\right) \frac{1 - \exp\left(-\Gamma \frac{x_1}{L}\right)}{\Gamma} \tag{41b}$$

and for

$$\xi_{\mathrm{I}} = \frac{\exp(\Gamma)(\Gamma - 1) + 1}{\Gamma (\exp(\Gamma) - 1)} , \quad \xi_{\mathrm{II}} = \xi_{\mathrm{I}} . \tag{42}$$

The idea of the power balance scheme is now to approximate the dynamic outlet temperatures $\vartheta^{\mathrm{out}}_{\mathrm{I}}$ and $\vartheta^{\mathrm{out}}_{\mathrm{II}}$ by θ_{I}, θ_{II}, $\vartheta^{\mathrm{in}}_{\mathrm{I}}$ and $\vartheta^{\mathrm{in}}_{\mathrm{II}}$ according to the stationary relationship of Eq. (39), i.e.

$$\vartheta^{\mathrm{out}}_{\mathrm{I}} = \frac{1}{\xi_{\mathrm{I}}} \theta_{\mathrm{I}} + \frac{\xi_{\mathrm{I}} - 1}{\xi_{\mathrm{I}}} \vartheta^{\mathrm{in}}_{\mathrm{I}} \tag{43a}$$

$$\vartheta^{\mathrm{out}}_{\mathrm{II}} = \frac{1}{\xi_{\mathrm{II}}} \theta_{\mathrm{II}} + \frac{\xi_{\mathrm{II}} - 1}{\xi_{\mathrm{II}}} \vartheta^{\mathrm{in}}_{\mathrm{II}} . \tag{43b}$$

Utilizing Eq. (43) the system matrices of Eq. (29) read as

$$\begin{gathered}
\mathbf{A} = \begin{bmatrix} -\frac{|\dot{m}_{\mathrm{I}}|}{m_{\mathrm{I}} \xi_{\mathrm{I}}} - \alpha_{\mathrm{I}} & \alpha_{\mathrm{I}} & 0 \\ \beta_{\mathrm{I}} & -(\beta_{\mathrm{I}} + \beta_{\mathrm{II}}) & \beta_{\mathrm{II}} \\ 0 & \alpha_{\mathrm{II}} & -\frac{|\dot{m}_{\mathrm{II}}|}{m_{\mathrm{II}} \xi_{\mathrm{II}}} - \alpha_{\mathrm{II}} \end{bmatrix} , \\
\mathbf{B} = \begin{bmatrix} \frac{|\dot{m}_{\mathrm{I}}|}{m_{\mathrm{I}} \xi_{\mathrm{I}}} & 0 \\ 0 & 0 \\ 0 & \frac{|\dot{m}_{\mathrm{II}}|}{m_{\mathrm{II}} \xi_{\mathrm{II}}} \end{bmatrix} , \quad \mathbf{C} = \begin{bmatrix} \frac{1}{\xi_{\mathrm{I}}} & 0 & 0 \\ 0 & 0 & \frac{1}{\xi_{\mathrm{II}}} \end{bmatrix} , \\
\mathbf{D} = \begin{bmatrix} 1 - \frac{1}{\xi_{\mathrm{I}}} & 0 \\ 0 & 1 - \frac{1}{\xi_{\mathrm{II}}} \end{bmatrix} .
\end{gathered} \tag{44}$$

Contrary to the upwind scheme, the power balance scheme ensures that the outlet temperatures stationary match the solution of the pde of Eq. (20) for $k_p = 0$.

Remark: Note that the power balance model Eq. (29), Eq. (44) is a finite-dimensional approximation of the distributed-parameter model Eqs. (20) – (22). The approximation scheme was designed in such a way that the resulting mathematical model exhibits a high stationary accuracy even for only $M = 1$ volume element. However, in case of very fast changes of the inlet temperatures the transient accuracy is limited due to the insufficient approximation of the transport phenomenon. In order to counteract this shortcoming, the number M of volume elements and thus the dimension of the power balance model has to be increased. As a rule of thumb, the residence time of the fluid inside a volume element should be smaller than the minimum rise time of the inlet temperatures.

Post-print version of the article: A. Michel and A. Kugi, "Accurate low-order dynamic model of a compact plate heat exchanger", *International Journal of Heat and Mass Transfer*, vol. 61, no. 33, pp. 323–331, 2013. DOI: 10.1016/j.ijheatmasstransfer.2013.01.072
The content of this post-print version is identical to the published paper but without the publisher's final layout or copy editing.

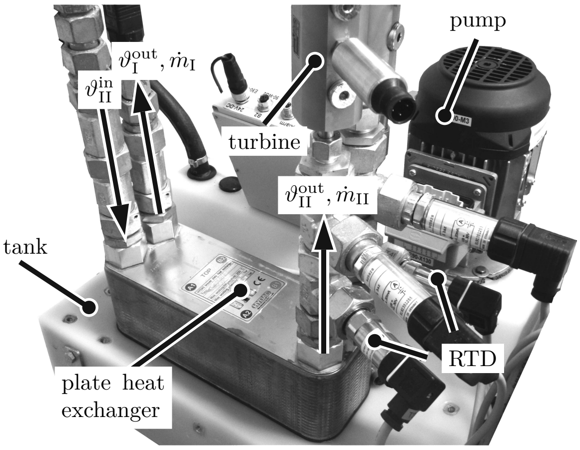

Figure 4: Photo of the test bed.

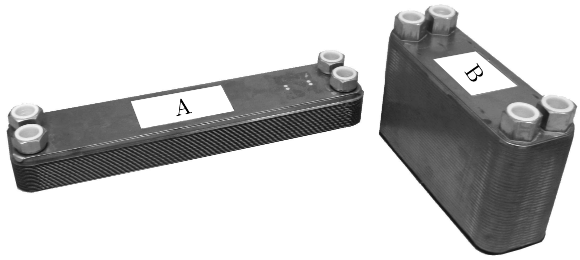

Figure 6: Examined plate heat exchangers.

Description	Symbol	A	B	Unit
channel length	L	46	25	cm
channel width	B	10.6	10.6	cm
channel height	H	2	1.8	mm
plate thickness	H_p	0.5	0.5	mm
number of plates	N_p	20	40	
correlation parameter	C_{Nu}	0.5	0.38	
correlation parameter	n_{Pr}	0.26	0.26	
correlation parameter	n_{Re}	0.67	0.68	
density (plate)	ϱ_p	8000	8000	kg/m^3
specific heat capacity (plate)	$c_{p,p}$	500	500	J/kg/K
thermal conductivity (plate)	k_p	15	15	W/m/K

Table 1: Parameter of the analyzed plate heat exchangers.

4. Validation of the proposed model

4.1. Experimental setup

In order to validate the presented mathematical models, a test bed was set up wherein two fluid circuits, one with a heater and one with a cooling system, are thermally coupled by a 1/1 pass countercurrent brazed plate heat exchanger in U-form. A picture of the test bed is shown in Figure 4 and the schematics are depicted in Figure 5. For

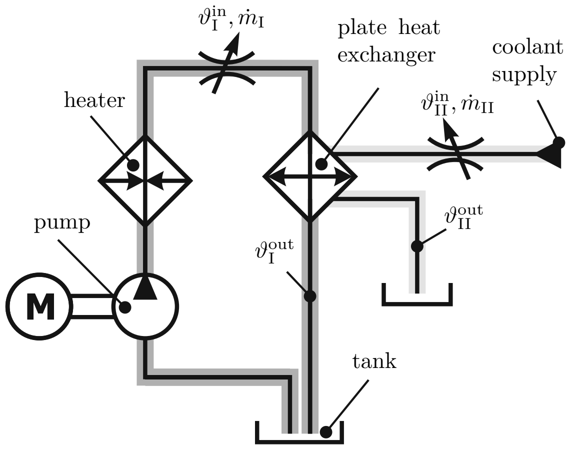

Figure 5: Schematic design of the test bed.

the experiments, two different designs of industrial plate heat exchangers have been used, see Figure 6, with the parameters listed in Table 1. The fluid I is a water-glycol mixture with 44% concentration. As coolant, water is used in experiment A and a water-glycol mixture with 40% concentration in experiment B. All fluid parameters with their temperature dependencies can be found in the relevant literature, see, e.g., [10]. Each flow is driven by a pump where the mass flow rates can be controlled by proportional valves. The inlet and outlet temperatures are measured by resistance thermometers (RTDs) and the two volume flow rates by means of turbine meters. The empirical parameters C_{Nu}, n_{Pr} and n_{Re} of Eq. (11) were identified by means of manufacturer's steady state data with the procedure explained in the following section.

4.2. Identification of the thermal coupling

As mentioned in Section 2, the parameters C_{Nu}, n_{Pr} and n_{Re} of Eq. (11) have to be determined by means of suitable experiments. Manufacturer often provide measurements of stationary outlet temperatures $\vartheta_{\mathrm{I},s}^{\mathrm{out},m}$, $\vartheta_{\mathrm{II},s}^{\mathrm{out},m}$ for different but constant mass flow rates $\dot{m}_{\mathrm{I},s}^{m}$, $\dot{m}_{\mathrm{II},s}^{m}$ and inlet temperatures $\vartheta_{\mathrm{I},s}^{\mathrm{in},m}$, $\vartheta_{\mathrm{II},s}^{\mathrm{in},m}$. These steady state data can be used in order to adapt the calculated stationary outlet temperatures $\vartheta_{\mathrm{I},s}^{\mathrm{out},c}$, $\vartheta_{\mathrm{II},s}^{\mathrm{out},c}$ to the measurements. Note that henceforth the added superscript m and c refer to measured and calculated variables, respectively.

Assuming countercurrent flow with $\dot{m}_{\mathrm{I}} > 0$ and $\dot{m}_{\mathrm{II}} < 0$, cf. Eq. (32), the stationary outlet temperatures can be

Post-print version of the article: A. Michel and A. Kugi, "Accurate low-order dynamic model of a compact plate heat exchanger", *International Journal of Heat and Mass Transfer*, vol. 61, no. 33, pp. 323–331, 2013. DOI: 10.1016/j.ijheatmasstransfer.2013.01.072
The content of this post-print version is identical to the published paper but without the publisher's final layout or copy editing.

calculated as,

$$\vartheta_{\mathrm{I},s}^{\mathrm{out},c} = \vartheta_{\mathrm{I},s}^{\mathrm{in},m} - \left(\vartheta_{\mathrm{I},s}^{\mathrm{in},m} - \vartheta_{\mathrm{II},s}^{\mathrm{in},m}\right) \frac{1-\exp(-\Gamma^c)}{1+\frac{\gamma_{\mathrm{II}}^c}{\gamma_{\mathrm{I}}^c}\exp(-\Gamma^c)} \tag{45a}$$

$$\vartheta_{\mathrm{II},s}^{\mathrm{out},c} = \vartheta_{\mathrm{I},s}^{\mathrm{in},m} - \left(\vartheta_{\mathrm{I},s}^{\mathrm{in},m} - \vartheta_{\mathrm{II},s}^{\mathrm{in},m}\right) \frac{1+\frac{\gamma_{\mathrm{II}}^c}{\gamma_{\mathrm{I}}^c}}{1+\frac{\gamma_{\mathrm{II}}^c}{\gamma_{\mathrm{I}}^c}\exp(-\Gamma^c)}\,, \tag{45b}$$

where the overall heat transfer coefficient U^c in γ_{I}^c, γ_{II}^c and Γ^c according to Eqs. (36), (19), (10) and (11) reads as

$$\frac{1}{U^c} = \frac{2H}{k_{\mathrm{I}} C_{Nu} Pr_{\mathrm{I}}^{n_{Pr}} Re_{\mathrm{I}}^{n_{Re}}} + \frac{2H}{k_{\mathrm{II}} C_{Nu} Pr_{\mathrm{II}}^{n_{Pr}} Re_{\mathrm{II}}^{n_{Re}}} + \frac{H_p}{k_p}\,. \tag{46}$$

For all stationary measurements the error between the measured and the calculated outlet temperatures $\vartheta_{\mathrm{I},s}^{\mathrm{out},m} - \vartheta_{\mathrm{I},s}^{\mathrm{out},c}$ and $\vartheta_{\mathrm{II},s}^{\mathrm{out},m} - \vartheta_{\mathrm{II},s}^{\mathrm{out},c}$ are combined in the error vectors $\mathbf{e}_{\mathrm{I}}$ and $\mathbf{e}_{\mathrm{II}}$, respectively. Then the parameters C_{Nu}, n_{Pr} and n_{Re} are determined by solving the nonlinear optimization problem

$$\min_{C_{Nu}, n_{Pr}, n_{Re}} w_{\mathrm{I}} \mathbf{e}_{\mathrm{I}}^T \mathbf{e}_{\mathrm{I}} + w_{\mathrm{II}} \mathbf{e}_{\mathrm{II}}^T \mathbf{e}_{\mathrm{II}} \tag{47}$$

for suitable weighting factors $w_{\mathrm{I}}, w_{\mathrm{II}} > 0$. In our case an interior-point method was employed utilizing the MATLAB function `fmincon`.

4.3. Measurement Results

For the experiments, the inputs, i.e. the two inlet temperatures $\vartheta_{\mathrm{I}}^{\mathrm{in}}$ and $\vartheta_{\mathrm{II}}^{\mathrm{in}}$ and the two mass flow rates $\dot{m}_{\mathrm{I}}$ and $\dot{m}_{\mathrm{II}}$, are varied over the operating range and are depicted in the left pictures of Figure 7 and Figure 8 for the two experiments A and B, respectively. These measured time evolutions also serve as inputs for the different mathematical models. The model accuracy is then assessed by comparing the resulting measured outlet temperatures $\vartheta_{\mathrm{I}}^{\mathrm{out}}$ and $\vartheta_{\mathrm{II}}^{\mathrm{out}}$ with the simulated ones. Thereby, two low-order mathematical models, each only with $M = 1$ volume element, based on the upwind and the power balance scheme according to Section 3.1 and Section 3.2, and two further higher order models employing the upwind scheme with $M = 10$ and $M = 100$ volume elements are used for comparison purposes. The time evolutions of the simulated and measured outlet temperatures $\vartheta_{\mathrm{I}}^{\mathrm{out}}$ and $\vartheta_{\mathrm{II}}^{\mathrm{out}}$ as well as the relative errors e_{I} and e_{II} of the simulation results are given in the right pictures of Figure 7 and Figure 8.

As expected, the errors of the upwind scheme models decrease for an increasing number of volume elements M. The mathematical model based on the power balance scheme already shows very good results for only one volume element ($M = 1$) and is comparable to the upwind scheme model with $M = 100$. Here the resulting stationary simulation error is less than 3% for experiment B and even less than 1% for experiment A. Larger deviations only occur for fast changing mass flow rates. At this point it is worth mentioning that already small errors in the parameters of the Nußelt correlation (given in Eq. (11)) or in the mass flow rates result in relative errors of the outlet temperatures in the percentage range. Thus, the quality of the low-order mathematical model with the power balance scheme can be rated very high, in particular if we take into account that the dynamics of the sensors was disregarded in the evaluation. The nearly perfect matching between the upwind scheme model with $M = 100$ and the power balance scheme model with $M = 1$ confirms the assumption that for compact plate heat exchangers the residence time of the fluid can be neglected. The only need for higher approximations within the upwind scheme is up to the nonlinear quasi-stationary behavior, which is inherently accounted for by the power balance scheme due to its specific construction.

5. Conclusion

Starting with a detailed modeling based on the fundamentals of heat transfer and the similitude theory according to Nußelt, a temperature mean value model consisting of three partial differential equations (pdes) was derived for a class of compact plate heat exchangers. A semi-discretization by means of the finite volume method was performed in order to obtain a model of ordinary differential equations. Due to the small fluid residence time and the limited dynamics of the inlet temperatures a discretization by only one single volume element was possible. The relation between the outlet temperatures and the states of the reduced model was established by the classical upwind and a newly developed power balance scheme. The latter was derived utilizing an approximate stationary solution of the underlying pdes. Finally, the models were validated by means of experimental results. It was shown that the mathematical model based on the power balance scheme with only one volume element exhibits similar high accuracy as the upwind scheme model with 100 volume elements. Since this low-order model succeeds in capturing the essential nonlinearities and the dynamic behavior in the considered operating range it serves as a suitable basis for model-based (nonlinear) control and optimization. Apart from the advantages of low complexity and high accuracy the model has the nice feature that the states are directly measurable and thus nonlinear state controllers may be directly applied without the need for a state observer. Note that this kind of low-order models can be applied to any kind of heat exchanger fulfilling the assumption of low fluid residence time compared to the dynamics of the inlet temperatures.

The stationary accuracy of the power balance scheme directly depends on the quality of the heat transfer model and thus on the identified correlation parameters. Because these parameters also appear as exponents in the Nußelt correlation, already small differences lead to high errors

Post-print version of the article: A. Michel and A. Kugi, "Accurate low-order dynamic model of a compact plate heat exchanger", *International Journal of Heat and Mass Transfer*, vol. 61, no. 33, pp. 323–331, 2013. DOI: 10.1016/j.ijheatmasstransfer.2013.01.072
The content of this post-print version is identical to the published paper but without the publisher's final layout or copy editing.

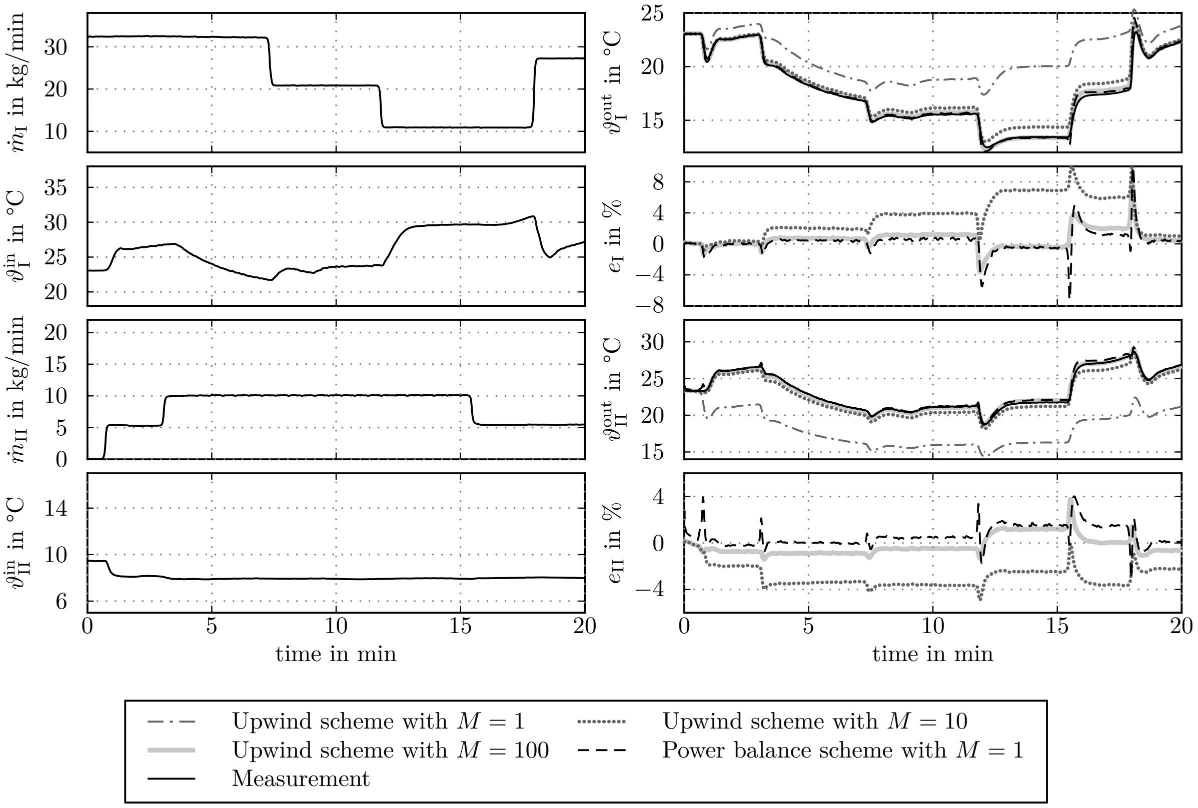

Figure 7: Measurement and simulation results for experiment A.

of the overall heat transfer coefficient and consequently to errors in the outlet temperatures. But this is not a drawback of the power balance scheme but will appear in every finite volume scheme based on the proposed Nußelt correlation. Moreover, the proposed power balance model with only one discretization element has its limitation. If the dynamics of the inlet temperatures are higher than the corresponding residence time of the fluid inside a discretization element, the transport phenomenon gets more dominant and a higher order finite volume model is indispensable. However, the power balance scheme is also applicable in this case, but the number of volume elements and hence the dimension of the resulting model has to be increased.

Acknowledgements

We highly appreciate the technical and financial support provided by Hydac Cooling GmbH, Germany.

References

[1] R. Shah, D. Sekulić, Fundamentals of Heat Exchanger Design, John Wiley & Sons, New Jersey, 2003.

[2] M. Masubuchi, A. Ito, Dynamic Analysis of a Plate Heat Exchanger System, Bulletin of the Japan Society of Mechanical Engineering 20 (1977) 434–441.

[3] S. Das, W. Roetzel, Dynamic Analysis of Plate Heat Exchangers with Dispersion in both Fluids, International Journal of Heat and Mass Transfer 38 (1995) 1127–1140.

[4] S. Das, B. Spang, W. Roetzel, Dynamic Behavouir of Plate Heat Exchangers - Experiments and Modeling, ASME Journal of Heat Transfer 117 (1995) 859–864.

[5] X. Luo, X. Guan, M. Li, W. Roetzel, Dynamic Behavouir of one-dimensional Flow Multistream Heat Exchangers and their Networks, International Journal of Heat and Mass Transfer 46 (2002) 705–715.

[6] J. Yin, M. Jensen, Analytical Model for Transient Heat Exchanger Response, International Journal of Heat and Mass Transfer 46 (2003) 3255–3264.

[7] F. Bechmann, Das stationäre und instationäre Verhalten von Platten-Wärmeübertragern im industiellen Maßstab, VDI Verlag, Düsseldorf, 1996.

[8] A. Dwivedi, S. Das, Dynamics of Plate Heat Exchangers Subject to Flow Variations, International Journal of Heat and Mass Transfer 50 (2007) 2733–2743.

[9] G. Jonsson, O. Palsson, Use of Emperical Relations in the Parameters of Heat-Exchanger Models, Industrial & Engineering Chemistry Research 30 (1991) 1193–1199.

[10] VDI-Gesellschaft Verfahrenstechnik und Chemieingenieurwesen, VDI Heat Atlas, Springer, Berlin/Heidelberg, 2. edition, 2010.

[11] M. Bassiouny, Expermientelle und theoretische Untersuchungen über Mengenstromverteilung, Druckverlust und Wärmeüber-

Post-print version of the article: A. Michel and A. Kugi, "Accurate low-order dynamic model of a compact plate heat exchanger", *International Journal of Heat and Mass Transfer*, vol. 61, no. 33, pp. 323–331, 2013. DOI: 10.1016/j.ijheatmasstransfer.2013.01.072
The content of this post-print version is identical to the published paper but without the publisher's final layout or copy editing.

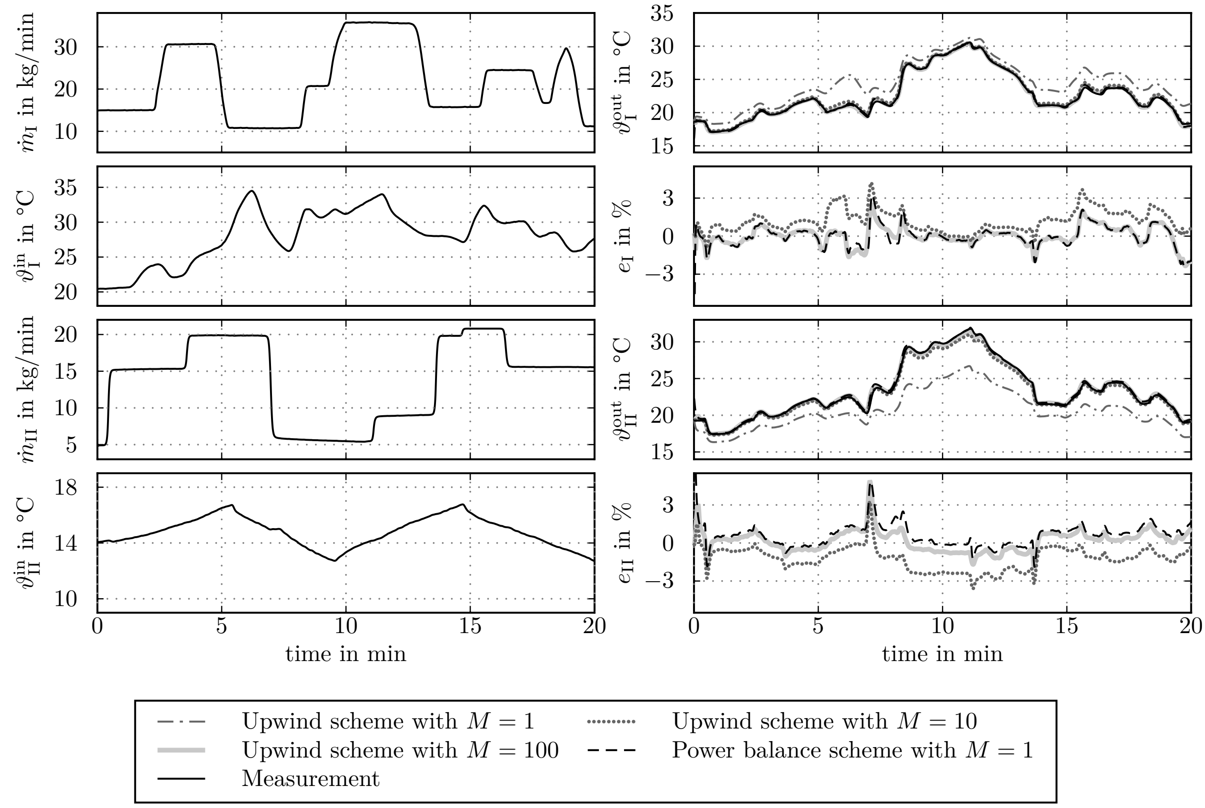

Figure 8: Measurement and simulation results for experiment B.

gang in Plattenwärmeaustauschern, VDI Verlag, Karlsruhe, 1985.

[12] W. Roetzel, Y. Xuan, Dynamic Behaviour of Heat Exchangers, WIT Press, Boston/Southampton, 1999.

[13] H. Baehr, K. Stephan, Heat and Mass Transfer, Springer, Berlin / Heidelberg, 2. edition, 2006.

[14] F. Incorpera, D. DeWitt, T. Bergman, A. Lavine, Fundamentals of Heat and Mass Transfer, John Wiley & Sons, US, 2007.

[15] J. Holman, Heat Transfer, McGraham-Hill, New York, 10. edition, 2010.

[16] R. Heavner, H. Kumar, A. Wanniarachchi, Performance of an Industrial Plate Heat Exchanger: Effect of Chevron Angle, in: Proceedings of the American Institute of Chemical Engineers Symposium Series, volume 89, Atlanta, GA, USA, pp. 262–267.

[17] S. Jain, A. Joshi, P. Bansal, A New Approach to Numerical Simulation of Small Sized Plate Heat Exchangers With Chevron Plates, ASME Journal of Heat Transfer 129 (2007) 291–297.

[18] H. Martin, A Theoretical Approach to Predict the Performance of Chevron-Type Plate Heat Exchangers, Chemical Engineering and Processing 35 (1996) 301–310.

[19] J. Ferziger, M. Perić, Computational Methods for Fluid Dynamics, Springer-Verlag, Berlin / Heidelberg, 3rd edition, 2002.

[20] R. LeVeque, Finite-Volume Methods for Hyperbolic Problems, Cambridge Texts in Applied Mathematics, Cambridge University Press, Cambridge, 2002.

[21] S.V. Patankar, Numerical Heat Transfer and Fluid Flow, New Hemisphere Publishing Corporation, USA, 1980.

Post-print version of the article: A. Michel and A. Kugi, "Accurate low-order dynamic model of a compact plate heat exchanger", *International Journal of Heat and Mass Transfer*, vol. 61, no. 33, pp. 323–331, 2013. DOI: 10.1016/j.ijheatmasstransfer.2013.01.072
The content of this post-print version is identical to the published paper but without the publisher's final layout or copy editing.